



Mantle tomography and its relation to temperature and composition

Frédéric Deschamps*, Jeannot Trampert

Department of Geophysics, Utrecht University, Budapestlaan 4, P.O. Box 80021, 3508 TA Utrecht, The Netherlands

Accepted 9 September 2003

Abstract

We propose a new method to constrain lateral variations of temperature and composition in the lower mantle from global tomographic models of shear- and compressional-wave speed. We assume that the mantle consists of a mixture of perovskite and magnesio-wüstite. In a first stage, we directly invert V_P and V_S anomalies for variations of temperature and composition, using the appropriate partial derivatives (or sensitivities) of velocities to temperature and composition. However, uncertainties in the tomographic models and in the sensitivities are such that variations in composition are completely unconstrained. Inferring deterministic distributions of temperature and composition being currently not possible, we turn to a statistical approach, which allows to infer several robust features. Comparison between synthetic and predicted ratios of the relative shear- to compressional-velocity anomalies indicates that the origin of seismic anomalies cannot be purely thermal, but do not constrain the amplitude of the variations of temperature and composition. We show that we can estimate these variations using histograms of the relative V_P and V_S anomalies at a given depth. We computed histograms for a large variety of cases and found that at the bottom of the mantle, variations in the volumic fraction of perovskite from -14 to 10% are essential to explain seismic tomography. In the mid-mantle, anomalies of perovskite are not required, but moderate variations (up to 6%) can explain the observed distributions equally well. These trade-offs between anomalies of temperature and composition cannot be resolved by relative velocity anomalies alone. An accurate determination of temperature and composition requires the knowledge of density variations as well. We show that anomalies of iron can then also be resolved.

© 2003 Elsevier B.V. All rights reserved.

Keywords: Shear velocity anomaly; Compressional velocity anomaly; Mantle temperature and composition

1. Introduction

One of the most challenging issues concerning the Earth's mantle is to infer its thermo-chemical structure. Variations of temperature and composition are closely related to mantle dynamics. There is little doubt that convection controls heat and mass transfers in the mantle, but the mode of mantle convection is still a matter of debate. The simplest model

is whole-mantle convection driven by a strong bottom thermal boundary layer. If, on the other hand, plate tectonics is the main mode of heat transfer in the mantle, the bottom thermal boundary layer is weak (Labrosse and Tackley, 2001). A variant of whole-mantle convection is the 'blob' model (Becker et al., 1999), in which residual blobs of the primitive reservoir are dispatched throughout the lower mantle. Models of chemically stratified mantle have gained an increasing interest. Kellogg et al. (1999) proposed a model in which a dense layer surrounds the core mantle boundary. This layer peaks around a depth

* Corresponding author. Tel.: +31-30-2525135.

E-mail address: deschamp@geo.uu.nl (F. Deschamps).

of 1600 km, and is locally deflected by downwelling slabs. Analogical experiments of thermo-chemical convection (Davaille, 1999) predict two regimes, depending on the density contrast. The doming regime occurs if the density contrast is lower than 1%, whereas for higher contrasts convection is organized in two layers. Whichever the model, it creates variations of temperature and composition seismology would like to map.

Global tomographic models of the Earth started to provide good quality maps of the lower mantle, independently for compressional (V_P) and shear (V_S) velocities (e.g., Su and Dziewonski, 1997; Masters et al., 2000; Ritsema and van Heijst, 2002). Despite these recent improvements, interpretation of tomographic models is not as straightforward. The main difficulty is that seismic velocities (and density) depend simultaneously on temperature, composition and pressure. Two different lines of enquiring have been proposed in the literature. Forte and Mitrovica (2001) directly inverted models of bulk sound (V_ϕ) and shear velocity anomalies for an effective temperature and composition using sensitivities they determined from existing literature. More often, studies are based on the analysis of the average of the distributions of the relative shear- to compressional-velocity anomalies (Karato and Karki, 2001, and references therein). A complicating factor in both approaches is that velocities alone cannot resolve all trade-offs between temperature and chemical variations. Density variations are needed in addition to velocity perturbations (e.g., Forte and Mitrovica, 2001; Karato and Karki, 2001).

In the present paper, we show that the deterministic approach of Forte and Mitrovica (2001) is not entirely robust given uncertainties, especially in the tomographic models. The approach based on the mean of the relative shear- to compressional-wave speed ratio (Karato and Karki, 2001) gives at best an indication of the presence of chemical heterogeneities. We propose a statistical approach, and show that the full distribution of relative velocity anomalies give robust bounds on temperature and composition.

2. Sensitivities of seismic velocities

Seismic velocity anomalies observed in the mantle can have several origins, the main contributions being

anomalies of temperature and composition. At the base of the mantle, partial melt, if present, could contribute significantly to seismic anomalies (e.g., Williams and Garnero, 1996; Revenaugh and Meyer, 1997). The relative contribution of each parameter can be written as the product of a partial derivative (hereafter called the sensitivity) of seismic velocities to this parameter, and of the amplitude of the variations of this parameter. Accounting for thermal (dT) and compositional (dC) anomalies, and for the presence of partial melt (dF), the relative seismic velocity anomalies can be written as

$$\begin{aligned} d \ln V_P &= \frac{\partial \ln V_P}{\partial T} dT + \frac{\partial \ln V_P}{\partial C} dC + \frac{\partial \ln V_P}{\partial F} dF, \\ d \ln V_S &= \frac{\partial \ln V_S}{\partial T} dT + \frac{\partial \ln V_S}{\partial C} dC + \frac{\partial \ln V_S}{\partial F} dF \end{aligned} \quad (1)$$

where the compositional term can be separated in several contributions, the most important being the variations of the volumic fractions of perovskite (dX_{pv}) and iron (dX_{Fe}). The ratio R of the relative shear to compressional seismic velocity is defined as

$$R \equiv \frac{d \ln V_S}{d \ln V_P} \quad (2)$$

where $d \ln V_S$ and $d \ln V_P$ are given by Eq. (1). R can be estimated from seismic tomography. Given the sensitivities of V_P and V_S , this ratio might give clues on dT , dC and dF .

Sensitivities of velocities to temperature and composition as a function of depth are calculated using mineral physics data and equation of state (EOS) modeling. We applied the method of Trampert et al. (2001) to an aggregate of perovskite ($MgSiO_3$) and magnesio-wüstite (MgO) throughout the lower mantle. Each mineral of the aggregate is heated up to the potential temperature and adiabatically compressed to the required pressure. Additionally to Trampert et al. (2001), we required that our EOS fit all existing ab initio data. No modification was needed to fit density and the bulk modulus, but we had to prescribe a cross-derivative to fit the shear modulus data of Oganov et al. (2001) and Marton and Cohen (2002). Details can be found in Deschamps and Trampert (2003). Interestingly, this modification does not significantly change the sensitivities compared to those of Trampert et al. (2001). To assess sensitivities to iron and calcium, we explicitly accounted for changes in

the volumic fraction of these elements. We neglected effects of anelasticity, which appear to only have a minor influence on temperature sensitivities in the lower mantle (Trampert et al., 2001; Brodholt et al., 2003). Ignorance of the potential temperature, average composition and on thermo-elastic parameters lead to uncertainties in the sensitivities. We varied these parameters within their possible ranges, allowing a large set of reference models (temperature, composition, thermo-elastic properties). The mean values of the sensitivities and their variances are estimated from the predicted models that fit PREM within 1%. Trampert et al. (2001) performed this test on mantle-averaged profiles for V_P , V_S and density. We prefer comparisons with PREM at each depth. The reason is that high values of the potential temperature (say $T_p = 2500$ K) may fit PREM in the lowermost mantle, but not in the mid-mantle. By allowing a different reference temperature and composition at each depth, we account for eventual non-adiabatic increases of temperature. To test if the reference model might influence the

results, we repeated most of the calculations with the reference model ak135 (Kennett et al., 1995), but did not find any significant differences.

Fig. 1a and b displays sensitivities of V_P (plain curves) and V_S (dashed curves) to temperature and volumic fraction of perovskite as a function of depth. Most of the input values of thermo-elastic parameters at ambient pressure are taken from the compilation of Trampert et al. (2001), where we added recent ab initio data (Table 1). Temperature, composition and pressure are varied according to Table 2, and the thermo-elastic properties are varied within their error bars (Table 1). This generated 10 million cases, from which 230 000 to 460 000 fit PREM within 1%, depending on the depth. The sensitivities to temperature are always negative, but their absolute values are decreasing with depth. The ratio R (Eq. (2)) associated with pure variations of temperature does not vary significantly with depth, and remains between 1.35 and 1.65. The sensitivity of V_P to volumic fraction of perovskite is positive throughout the lower mantle,

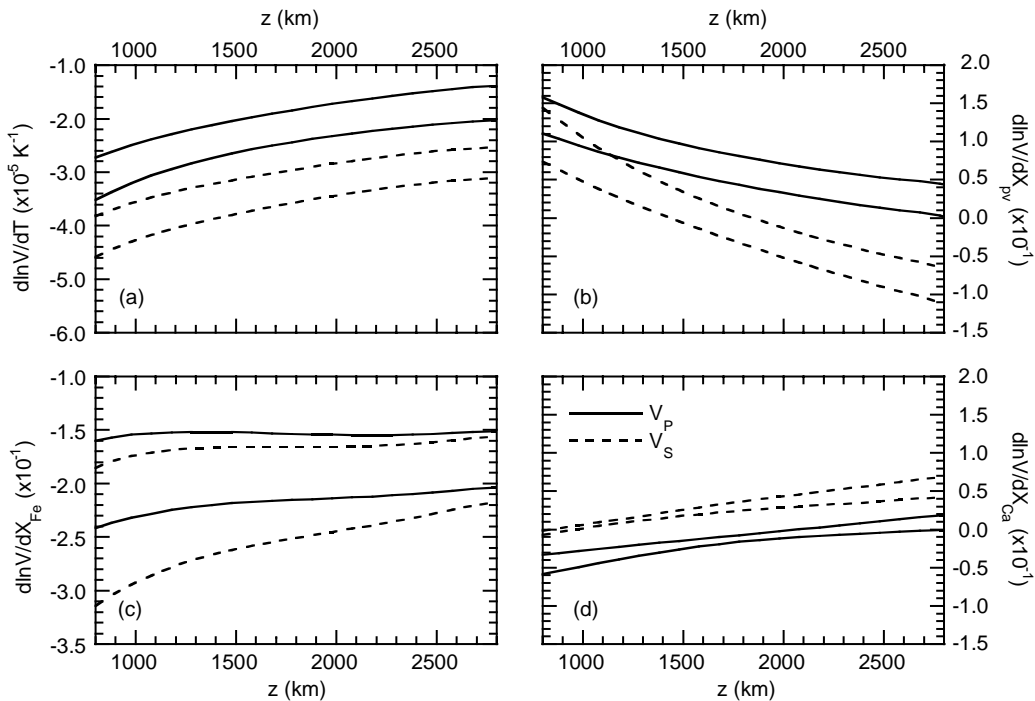


Fig. 1. Sensitivities of compressional velocity (plain curves) and shear velocity (dashed curves) to (a) temperature, (b) perovskite, (c) iron, and (d) calcium as a function of depth. In each case, we represent the upper and lower value of the sensitivity, which correspond to 1 standard deviation around the average. Averages and standard deviations are calculated from the predicted models that fit PREM within 1%.

Table 1
Thermoelastic properties of MgSiO₃ and MgO^a

	Perovskite	Magnesio-wüstite
ρ (g/cm ³)	4.109 + 1.03 X_{Fe}	3.584 + 2.28 X_{Fe}
K_{S0} (GPa)	264.0	162.5 + 11.5 X_{Fe}
K'_{S0}	3.97/3.95/3.77/3.75 ^b	4.0 ^c to 4.15 ^d
\dot{K}_{S0} (GPa/K)	-0.011/-0.015/ -0.010/-0.015 ^b	-0.0155 ^e to -0.014 ^d
G_0 (GPa)	180.0 ^f	130.8–75.6 X_{Fe}
G'_0	1.5 (0.05) ^g	2.4 ^c to 2.5
\dot{G}_0 (GPa/K)	-0.020 (0.008) ^h	-0.024 to -0.022 ^d
γ_0	1.31/1.39/1.33/1.41 ^b	1.41
q	1.0/2.0/1.0/2.0 ^b	1.3
a_1 (10 ⁻⁵ K ⁻¹)	1.19 (0.17)	3.681
a_2 (10 ⁻⁸ K ⁻²)	1.20 (0.10)	0.9283
a_3 (K)	0.0	0.7445

^a All data are from the compilation of Trampert et al. (2001) unless otherwise stated. When available, error bars are indicated in parenthesis. ρ is the density, K_{S0} the adiabatic bulk modulus, G_0 the shear modulus, γ_0 the Grüneisen parameter at ambient temperature and pressure, and q a constant. Primes and dots denote derivation with respect to pressure and temperature, respectively. To model the shear modulus of perovskite we prescribed a cross derivative, as suggested in Deschamps and Trampert (2003). This cross-derivative is given by $\partial^2 G / \partial T \partial P = c_1 (\dot{G}_0)_{\text{pv}} + c_2$, where $c_1 = -1.2 \times 10^{-2} \text{ GPa}^{-1}$ and $c_2 = -3.3 \times 10^{-4} \text{ K}^{-1}$. Thermal expansion is calculated following $\alpha = a_1 + a_2 T - a_3 T^{-2}$.

^b Following Jackson (1998), we consider four alternative combinations of K'_{S0} , \dot{K}_{S0} and γ_0 , depending on the values of K'_{T0} and q .

^c Sinogeikin and Bass (1999).

^d Karki et al. (2000).

^e Sumino et al. (1983).

^f Oganov et al. (2001).

^g We used the value of \dot{G}_0 proposed by Jackson (1998). The error bar accounts for the ab initio data of Marton and Cohen (2002), and the experimental data of Sinelnikov et al. (1998).

^h Value giving the best fit to ab initio data of Oganov et al. (2001) at room temperature. Note that this value is close to the experimental lower bound (Sinelnikov et al., 1998).

whereas the mean sensitivity of V_S to volumic fraction of perovskite gets negative at a depth of about 1600 km. Therefore, the ratios R associated with pure variations of perovskite are negative in a large part of the lower mantle. We have explicitly calculated sensitivities to the global volumic fraction of iron, X_{Fe} (Fig. 1c). This parameter is given by

$$X_{\text{Fe}} = X_{\text{pv}} x_{\text{Fe}}^{\text{pv}} + (1 - X_{\text{pv}}) x_{\text{Fe}}^{\text{mw}} \quad (3)$$

where X_{pv} is the volumic fraction of perovskite. The volumic fractions of iron in perovskite ($x_{\text{Fe}}^{\text{pv}}$) and in magnesio-wüstite ($x_{\text{Fe}}^{\text{mw}}$) can be calculated from X_{Fe}

Table 2
Variations of temperature, pressure and composition^a

Parameter	Minimal value	Maximal value
T_p (K)	1500	3000
X_{pv}	0.5	1.0
X_{Fe}	0.05	0.15
X_{Ca}	0.0	0.15
K_{Fe}	0.2	0.5
P/P_{PREM}	0.99	1.01

^a T_p is the potential temperature, X_{pv} the volumic fraction of perovskite, X_{Fe} the global volumic fraction of iron, X_{Ca} the global volumic fraction of calcium, K_{Fe} the iron partitioning, and P the pressure.

using the relation (3), and the definition of the iron partitioning between perovskite and magnesio-wüstite,

$$K_{\text{Fe}} = \frac{x_{\text{Fe}}^{\text{pv}} / (1 - x_{\text{Fe}}^{\text{pv}})}{x_{\text{Fe}}^{\text{mw}} / (1 - x_{\text{Fe}}^{\text{mw}})} \quad (4)$$

Sensitivities to iron content are negative throughout the mantle, for both V_p and V_S . Within uncertainties, they are very close one another, at any depth. As a consequence, for pure anomalies of iron, values of R are close to 1.0, varying between 1.1 and 1.3 with depth. Because these values are close to those for pure anomalies of temperature, R cannot discriminate between anomalies of temperature and iron. On the other hand, R is useful to detect anomalies of perovskite, since pure anomalies of perovskite result in negative R in a large part of the lower mantle.

Calcium perovskite could also enter the composition of the lower mantle and influence the density and elastic moduli of the mantle aggregate. We used experimental measurements (Wang et al., 1996) and ab initio data (Karki and Crain, 1998), and found that the sensitivities of seismic velocities to calcium are small compared to other compositional parameters (Fig. 1d). On average, they are smaller than the sensitivities to iron by one order of magnitude. If, as expected, Ca-Perovskite enters the composition of the lower mantle for 6–12% in volume, the effects on seismic velocities would be of second order compared to other compositional parameters. For instance, a 12% anomaly of Ca-Perovskite at the bottom of the mantle would give relative anomalies of V_p and V_S of 0.1 and 0.2%, respectively. Aluminium perovskite, which is also expected to be present in the lower mantle, may have more dramatic effects, but very few data

(experimental or *ab initio*) are available. So far, we could not calculate robust sensitivities to aluminium and investigate its effects.

Sensitivities to partial melt are more delicate to estimate. A difficulty is that they strongly depend on the geometry of the melt (Hammond and Humphreys, 2000). Berryman (2000), however, suggested that the ratio R associated with partial melt does not depend on the melt geometry, and has a value close to 3. The values of sensitivities proposed by Hammond and Humphreys (2000) for the upper mantle may not be relevant at lower mantle pressure. Best estimates of sensitivities to partial melt are inferred from seismic studies of the base of the mantle. Williams and Garnero (1996) proposed values of $d \ln V_P$ ($d \ln V_S$) between -0.4 and -1.4% (-1.0 and -4.3%) for 1% of partial melt, depending on the melt geometry. These values agree with the assumption that $R \sim 3$ whatever the geometry (Berryman, 2000). According to Williams and Garnero (1996), partial melt is present in a volume of 5–40 km thickness, with a lateral surface of $20 \times 20^\circ$. Revenaugh and Meyer (1997), on another hand, invoke the presence of partial melt in a simple 15 km thick layer above the core–mantle boundary to explain observed PcP travel time residuals. Global tomographic models cannot yet resolve fine vertical structures. In global models, the effects of partial melt are therefore diluted, and a correction must be applied. The vertical resolution of global models of V_P and V_S (Masters et al., 2000; Ritsema and van Heijst, 2002) is 10 to 30 times larger than the thickness of pockets of partial melt. Accounting for this dilution, realistic values of the sensitivities of V_P and V_S per percent of partial melt are $d \ln V_P = -0.03$ to -0.1% , and $d \ln V_S = -0.1$ to -0.3% , respectively.

3. Direct inversion of global compressional- and shear- velocity anomalies

A straightforward approach to infer thermal and compositional variations in the mantle is to invert relative V_P and V_S anomalies ($d \ln V_P$ and $d \ln V_S$) directly using Eq. (1). Since there are only two data constraints, composition is represented by one single parameter, and partial melt is neglected. Chemically stratified models of convection (Davaille, 1999; Kellogg

et al., 1999) have assumed the presence of a denser layer at the bottom of the mantle. Because perovskite is denser than magnesio-wüstite, a dense layer at the bottom could be significantly enriched in perovskite. Note that the accumulation of cold slabs issued from oceanic lithosphere would result in a depletion in perovskite, because harzburgite is preferentially transformed in magnesio-wüstite (Ringwood, 1991). A denser layer can also be explained by an excess of iron that could result from local contaminations from the outer core at the core–mantle boundary (Knittle and Jeanloz, 1991; Garnero and Jeanloz, 2000). As suggested by the analysis of R for pure variations of temperature, perovskite and iron, V_P and V_S anomalies can only distinguish between temperature and perovskite. Iron trades off completely with temperature, and we have neglected it here.

We used the $d \ln V_P$ and $d \ln V_S$ from the model SB10L18 (Masters et al., 2000) and assumed in a first stage that there are no errors in the model. This model consists of 18 layers, and each layer is divided into blocks of equal area, with a dimension of 4° at the equator. It is straightforward to invert $d \ln V_P$ and $d \ln V_S$ in each block for dT and dX_{pv} . We varied the sensitivities of seismic velocities according to their possible range, randomly generating sensitivities to temperature and perovskite with a Gaussian probability distribution (e.g. Press et al., 1989, pp. 191–203). The mean and standard deviation of the distribution at each depth are those displayed in Fig. 1a and b. This resulted in a collection of models for the anomalies of temperature and perovskite. The mean values of dT and dX_{pv} in each block are displayed in Figs. 2a and c and 3a and c at depths of $z = 1400$ km and $z = 2800$ km. We do not observe any prominent features at $z = 1400$ km depth (Figs. 2a and 3a). At this depth, the mantle seems relatively homogeneous (small temperature and perovskite variations). Anomalies of perovskite and temperature are distributed with a standard deviation equal to 3.7% and 190 K, respectively. At $z = 2800$ km depth, we clearly identify two regions of material enriched in perovskite (Fig. 3c). One is located beneath the Pacific, and the other one beneath Africa. Both are well correlated with positive anomalies of temperature (Fig. 2c). Regions strongly depleted in perovskite correspond to those of the circum-Pacific belt. In addition, anomalies of temperature and perovskite are here more pronounced than

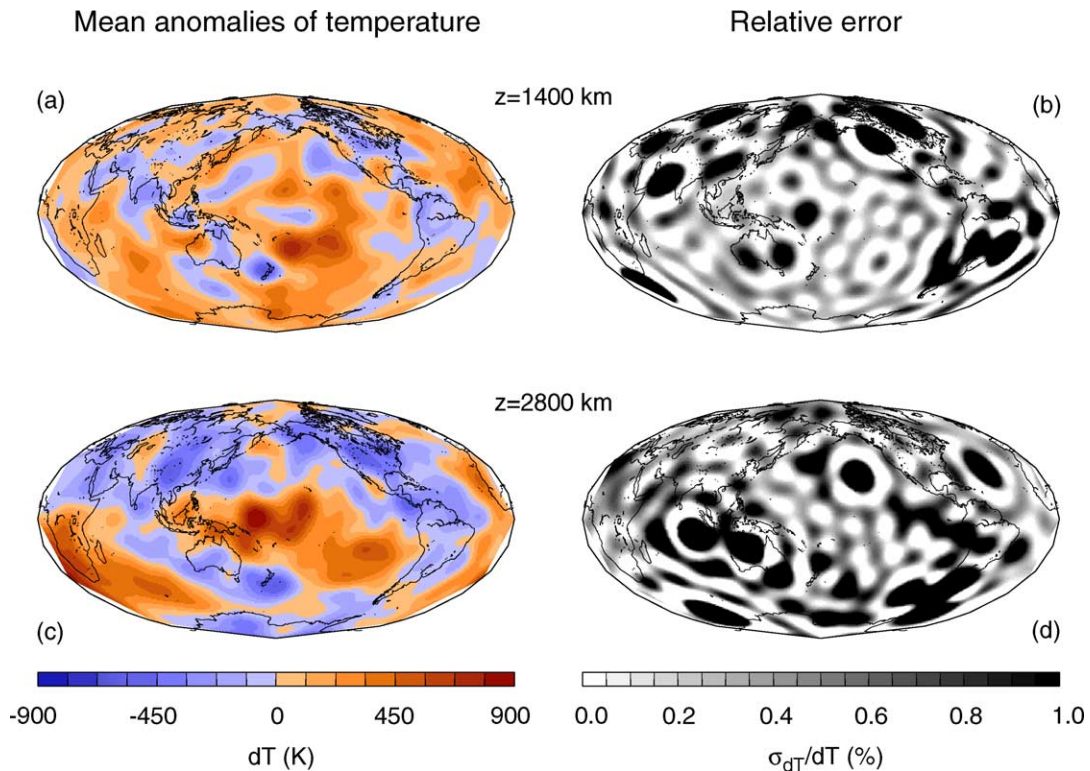


Fig. 2. Anomalies of temperature (a and c) and their relative errors (b and d) obtained with the tomographic model SB10L18 (Masters et al., 2000) at (a–b) $z = 1400$ km and (c–d) $z = 2800$ km. Relative errors are due to uncertainties in the sensitivities of seismic velocities to temperature (Fig. 1a). Maps are filtered for spherical harmonic degrees $\ell = 0$ to $\ell = 18$.

in the mid-mantle. Anomalies of perovskite (temperature) locally reach values of 12% (900 K), and the standard deviation of the distribution is 5.1% (270 K). Our results agree remarkably well with those of Forte and Mitrovica (2001), who have computed ‘effective’ anomalies of composition and temperature (i.e., anomalies of perovskite and temperature, including anomalies of iron) from different tomographic models and with independently calculated sensitivities.

The burning question is to know how robust these inferences are. Uncertainties on dT and dX_{pv} are due to uncertainties on the tomographic models and on the sensitivities of seismic velocities to temperature and perovskite (Fig. 1a and b). Figs. 2b and d and 3b and d display the local relative errors in temperature and perovskite due to uncertainties in the sensitivities alone (errors in tomography are for the moment neglected). The relative errors are defined as the standard deviation over the mean estimated from the collec-

tion of anomalies of temperature and perovskite. Variations of temperature are relatively well constrained (Fig. 2b and d), although the relative error is close to 1.0 in some small regions. The root mean square (R.M.S.) of the relative error in temperature at each depth remains around 0.2 between $z = 1200$ km and the CMB (Fig. 4a, curve labeled 0.0). In the top layer of the lower mantle, the R.M.S. is higher, up to 0.5 at $z = 800$ km. The distributions of perovskite are much more poorly constrained (Fig. 3b and d). Between $z = 1200$ km and the CMB, the R.M.S. of the relative error for perovskite is close to 0.45, and it reaches 0.77 at $z = 800$ km (Fig. 4b, curve labeled 0.0). These errors can be viewed as conservative because only 67% of the obtained models fall within 1 standard deviation. Further, we need to include errors in the tomographic models themselves. Because tomographic models do not generally provide uncertainties, we have simulated random errors in $d \ln V_p$ and $d \ln V_s$ using Gaussian

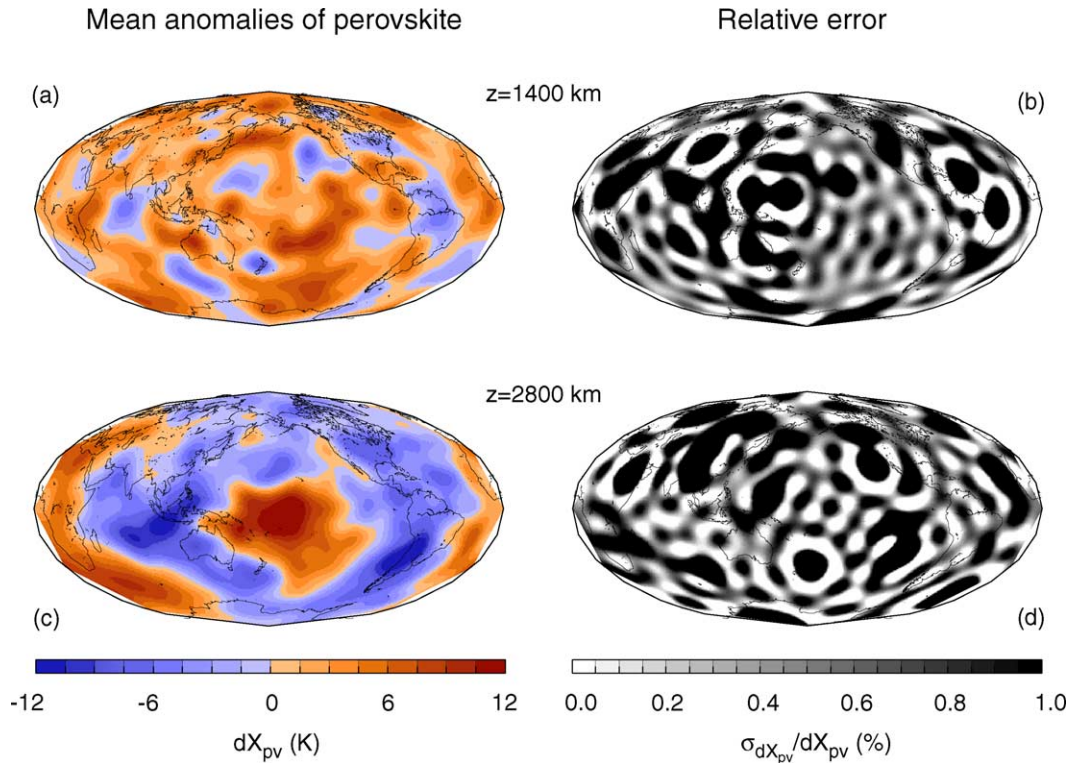


Fig. 3. Anomalies of perovskite (a and c) and their relative errors (b and d) obtained with the tomographic model SB10L18 (Masters et al., 2000) at (a–b) $z = 1400$ km and (c–d) $z = 2800$ km. Relative errors are due to uncertainties in the sensitivities of seismic velocities to perovskite (Fig. 1b). Maps are filtered for spherical harmonic degrees $\ell = 0$ to $\ell = 18$.

statistics. We simulated inversions with increasing relative error in the tomographic models, generating each time a collection of models for anomalies of temperature and perovskite. In each case, we calculated the mean and standard deviation in each block, and then computed the R.M.S. of the relative error in dT and dX_{pv} as a function of depth (Fig. 4). As previously, the sensitivities are varied within their ranges shown in Fig. 1. The R.M.S. relative error on perovskite increases very rapidly with increasing error in tomography, and becomes bigger than 1 for relative errors of the velocity anomalies close to 0.4 (Fig. 4b). A R.M.S. relative error bigger than 1 means that the average error exceeds the average signal and the inference is not robust. The R.M.S. relative error on temperature also increases with depth, but much slower. Temperature remains robust at most depths.

It is not unreasonable to assume relative errors in velocity anomalies in excess of 0.3 as has been found by directly comparing several tomographic models

(Resovsky and Ritzwoller, 1999), or by full model space search (Beghein et al., 2002). Deterministic inferences of composition obtained from a direct inversion of Eq. (1) are thus not robust at present, and temperature estimates contain at least 50% errors.

Using relative V_ϕ anomalies ($d \ln V_\phi$) instead of relative V_p anomalies results in smallest relative errors on temperature and composition. V_ϕ anomalies, however, are not inferred directly from seismic data, but are constructed from V_p and V_s . As a consequence, relative errors in $d \ln V_\phi$ are roughly twice the relative errors in $d \ln V_p$ and $d \ln V_s$, and the final conclusion would be the same.

4. Constraints from the ratio of relative shear to compressional velocity

The ratio R of the relative V_s anomalies to the relative V_p anomalies (Eq. (2)) is often used to

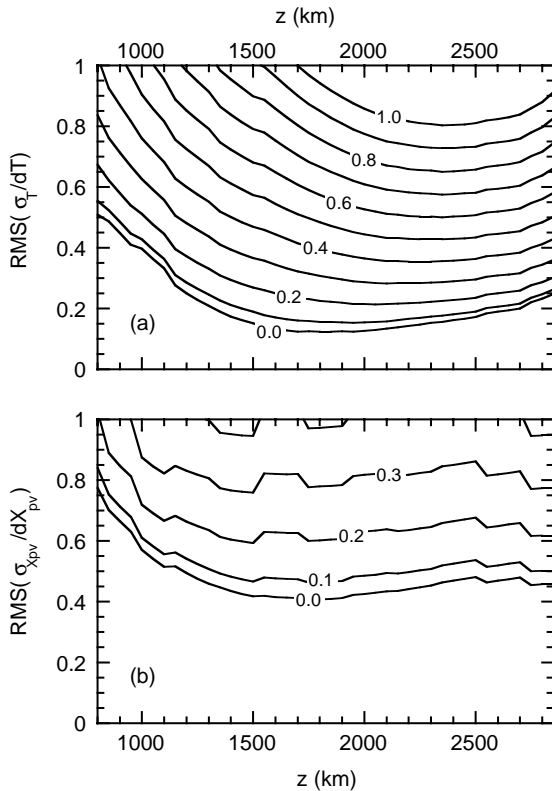


Fig. 4. Root mean square relative error in the anomalies of (a) temperature and (b) perovskite as a function of depth. In addition to the uncertainties in the sensitivities of seismic velocities, we modelled Gaussian errors in the relative V_P and V_S anomalies. The assumed relative errors are indicated on each curve.

scale compressional velocity from shear velocity as a function of depth in global tomographic models. If one has access to independent $d \ln V_P$ and $d \ln V_S$, R can be used as a diagnostic of the origin of these anomalies. Using P and S travel time residuals, Robertson and Woodhouse (1997) found $R = 1.58$ for the upper mantle. Masters et al. (2000) have recently compared average profiles of R for several joint models of V_P and V_S anomalies. All of them show significant variations with depth. In particular, the models of Su and Dziewonski (1997) and the model SB10L18 (Masters et al., 2000) show an increase of R with depth. For SB10L18, they found $R = 1.62$ at $z = 1400$ km, and $R = 2.52$ at $z = 2800$ km. On the basis of median values, Masters et al. (2000) proposed a thermal origin for the anomalies of velocity,

except for areas beneath the Pacific and Africa at the very bottom of the mantle, where they found that ratios are different. Saltzer et al. (2001) also clearly observed laterally varying values. Full histograms of block-by-block estimates of R clearly provide more information about the lateral variations of R at a given depth. We have computed ratios for each block of the models SB10L18 (Masters et al., 2000) and 12RTS (Ritsema and van Heijst, 2002), and binned them (Fig. 5). Note that very small values in the denominator give high values of the ratio if not balanced by small values of the $d \ln V_S$. We selected blocks for which the absolute value of the ratio is smaller than 10. Most blocks satisfy this condition (355 out of 408 for SB10L18 at $z = 2800$ km). The important feature is that histograms do not peak sharply around the mean value of R , but show significant dispersion. It is interesting to note that the dispersion is more important at the bottom of the mantle.

Fig. 6 shows histograms of the relative frequency of R obtained for pure variations of temperature (plain curves), perovskite (dotted curves) and iron (dashed curves). We constructed these histograms by varying the sensitivities of seismic velocities within their uncertainties (Fig. 1). For each individual case, a value of R is computed and binned. Due to uncertainties in the sensitivities, R will be dispersed even if one considers pure variations of one single parameter. Pure variations of temperature give values of R close to 1.6, regardless of the depth. The dispersion is very small (the standard deviation is around 0.2) and increases slightly with depth. Pure variations of iron lead to similar distributions. The mean value of R varies between 1.1 and 1.3, depending on the depth, with a standard deviation of about 0.2. Pure variations of perovskite show a very different behavior. At the top of the lower mantle ($z = 700$ km), they give values of R around 0.9, with a small dispersion. Dispersion then increases dramatically with depth, and the mean value of R shifts towards negative values. At the bottom of the lower mantle, the mean value of R is -4.1 and its standard deviation 2.0.

It is clear, from these results, that purely thermal or purely compositional anomalies cannot explain the observed histograms (Fig. 5). Rather, a mix of several effects, including uncertainties in the tomographic models, is responsible for the observed dispersion of histograms. At close inspection of Eq. (2), it becomes

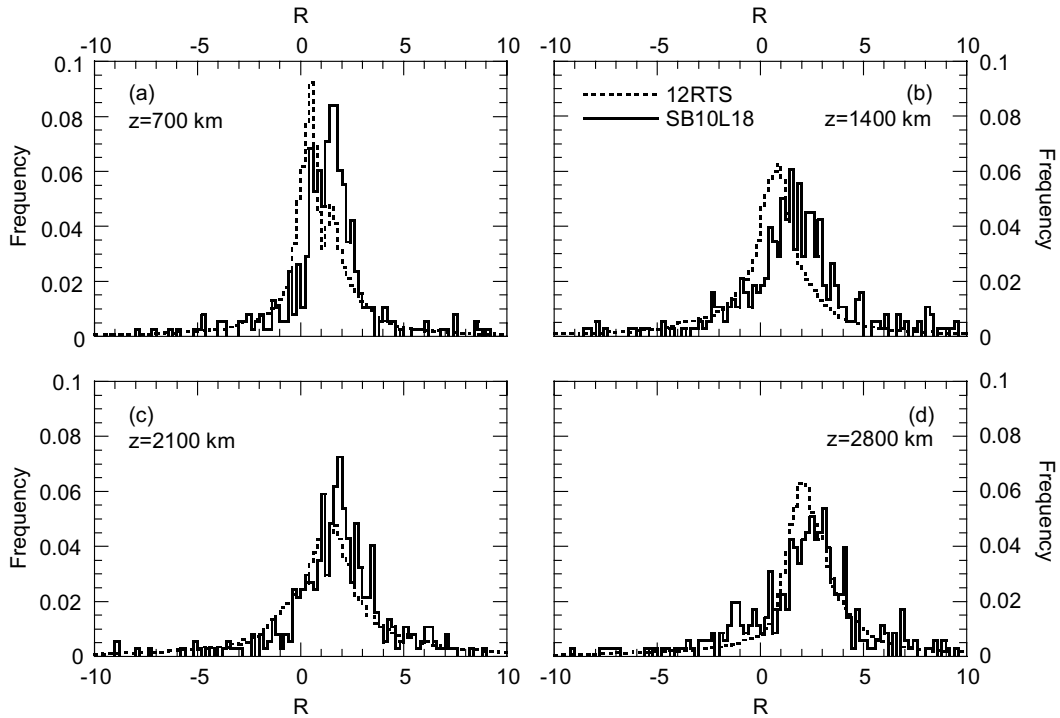


Fig. 5. Histograms of $R = d \ln V_S / d \ln V_P$ as a function of depth, and for two global models of V_P and V_S anomalies. Plain and dotted curves correspond to the models SB10L18 (Masters et al., 2000) and 12RTS (Ritsema and van Heijst, 2002), respectively. Depths represented are (a) $z = 700$ km, (b) $z = 1400$ km, (c) $z = 2100$ km and (d) $z = 2800$ km.

clear that the histograms of R cannot provide any quantitative statement about the bounds of dT and dC . Indeed, any scaling $\alpha dT + \alpha dC$ will result in the same R , meaning that the amplitude of the cause remains undetermined. The histograms however contain the important qualitative information that temperature alone cannot be responsible for the observed tomographic maps.

5. Robust constraints from the observed velocity anomalies

The ambiguity found in the interpretation of R is lifted if the velocity anomalies are analysed directly. The idea is that the bounds of dT , dC and dF are responsible for the shape of the observed histograms of $d \ln V_P$ and $d \ln V_S$. Using the sensitivities calculated in Section 2 together with Eq. (1), we generated synthetic values of velocity histograms for given ranges for dT , dC and dF , and compared them to the results of

tomography. To make robust comparisons, we need to include possible errors in tomography. In the synthetic histograms, we have simulated these errors by adding a term on the right hand side of Eq. (1). The errors are drawn in a Gaussian distribution with a standard deviation $\Delta(d \ln V_P)$ and $\Delta(d \ln V_S)$ (Table 3). This standard deviation is obtained by multiplying the R.M.S. amplitude of SB10L18 by a relative error. The relative error is taken from a full model space search applied to normal mode and surface wave data (Beghein et al., 2002). Although SB10L18 also contains body wave data, the relative errors of Beghein et al. (2002) are in good agreement with direct comparisons of different tomographic models (Resovsky and Ritzwoller, 1999), and thus represent the currently best estimates of errors in global tomographic models.

We made a systematic search for bounds in temperature and composition. For each obtained synthetic histogram, we computed the variance reduction with respect to the observed histogram. A selection of combinations is listed in Table 4, and some histograms are

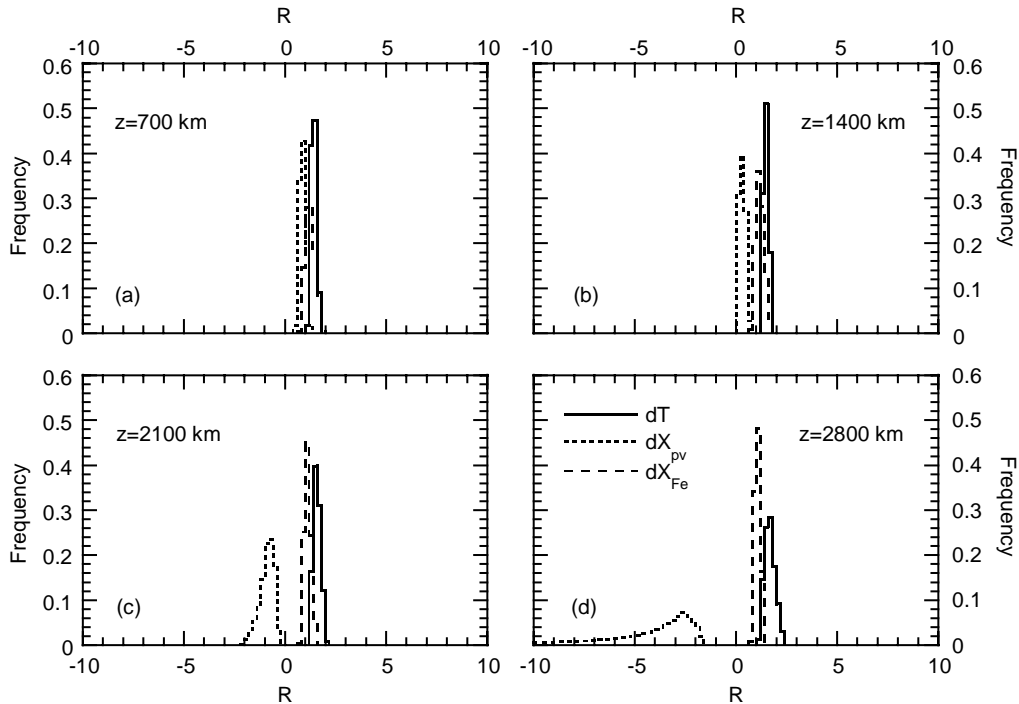


Fig. 6. Histograms of $R = d \ln V_S / d \ln V_P$ for different causes. Plain, dotted and dashed curves correspond to pure variations of temperature, perovskite, and iron, respectively. Depths represented are (a) $z = 700$ km, (b) $z = 1400$ km, (c) $z = 2100$ km and (d) $z = 2800$ km.

drawn in Fig. 7 (thick red curves) and compared to the observed ones (thin black curves). In the top and mid-lower mantle, moderate (up to 300 K) anomalies of temperature explain the observed histograms without the need of compositional anomalies (combinations 1, 6 and 11). For both $d \ln V_P$ and $d \ln V_S$, synthetic histograms fit observed histograms with a variance reduction higher than 89%. Other combinations, and in particular asymmetric combinations (e.g., 2, 7 and 12), fit observations less well. V_P and V_S

anomalies therefore provide good constraints on the temperature range. Moderate (up to 6%) anomalies in the volumic fraction of perovskite also give good fits to the observed histograms (e.g., combinations 3, 9 and 13), but larger variations (8% and more) fail to explain histograms for $d \ln V_P$ (e.g., combinations 5, 10 and 14, Fig. 7b, d and f). Variations in the volumic fraction of iron up to 2% do not significantly change the variance reduction, and are therefore consistent with the observations. At the bottom of the mantle,

Table 3
Errors $\Delta(d \ln V)$ on the relative anomalies of seismic velocities^a

Depth (km)	V_P			V_S		
	R.M.S. (10^{-3})	Relative errors	$\Delta(d \ln V)$ (10^{-3})	R.M.S. (10^{-3})	Relative errors	$\Delta(d \ln V)$ (10^{-3})
700	1.2	0.35	0.42	2.2	0.62	1.36
1400	0.7	0.65	0.46	1.7	0.31	0.53
2100	1.5	0.50	0.75	3.2	0.36	1.15
2800	1.7	0.78	1.33	6.2	0.56	3.47

^a The $\Delta(d \ln V)$ are computed from the R.M.S. amplitude of SB10L18 (Masters et al., 2000), and the relative errors from Beghein et al. (2002).

Table 4
Selected best combinations of thermal and compositional anomalies^a

No.	dT (K)		dX _{Pv} (%)		dX _{Fe} (%)		dF (%)	χ _P (%)	χ _S (%)
	Min	Max	Min	Max	Min	Max			
<i>z</i> = 700 km									
1	−300	300	0	0	0	0	0	93.0	89.4
2	−100	300	0	0	0	0	0	57.9	48.3
3	−300	300	−6	4	−2	2	0	90.1	91.1
4	−300	300	−12	6	0	0	0	72.3	81.6
5	−300	300	−12	6	−2	3	0	66.8	82.1
<i>z</i> = 1400 km									
6	−200	300	0	0	0	0	0	89.6	90.2
7	−100	400	0	0	0	0	0	67.2	77.2
8	−200	300	−4	6	0	0	0	91.0	89.8
9	−200	300	−4	6	−1	1	0	90.0	90.5
10	−200	300	−6	12	0	0	0	75.8	88.4
<i>z</i> = 2100 km									
11	−300	300	0	0	0	0	0	92.8	93.0
12	−300	100	0	0	0	0	0	47.2	39.1
13	−300	300	−6	2	−2	2	0	85.9	90.9
14	−300	300	−6	12	−2	2	0	71.9	93.6
<i>z</i> = 2800 km									
15	−400	400	0	0	0	0	0	94.3	59.6
16	−400	400	−14	6	0	0	0	93.6	81.9
17	−400	400	0	0	−3	3	0	94.1	65.6
18	−400	400	−14	6	−1	2	0	88.5	81.1
19	−400	400	−6	4	−1	2	0	92.4	65.0
20	−500	350	−14	10	−1	2	0	94.7	82.5
21	−500	350	−6	12	−1	2	0	85.8	72.7
22	−500	350	−14	6	−1	2	0	94.7	81.7
23	−500	350	−10	10	−1	2	0	94.0	78.0
24	−500	350	−10	14	−1	2	0	92.1	73.1
25	−500	350	−14	10	0	3	0	88.3	79.1
26	−500	350	−14	10	−3	0	0	61.2	76.9
27	−350	500	−14	10	−1	2	0	81.1	70.0
28	−600	300	−12	6	−1	2	0.1	94.5	80.4

^a Each case is defined by the minimal and maximal values of the anomalies of temperature (dT) and composition (dX_{Pv} and dX_{Fe}), and by the rate of partial melt (dF). χ_P and χ_S are the output variance reduction in respect with the histograms of V_P and V_S anomalies predicted by SB10L18.

temperature variations alone do not fit the observed d ln V_S histograms (combination 15, Fig. 7g). The origin of velocity anomalies can thus not be purely thermal. The compositional component is also not fully explained by variations in the volumic fraction of iron (combination 17). Furthermore, moderate (up to 6%) variations in perovskite do not fit the observation, even if variations in iron are considered (combination 19). Large variations of perovskite, with depletion (enrichment) up to 14% (10%), are required to explain the observed histogram of d ln V_S (e.g., combinations 16, 18 and 20). A large number of combinations

explain the observed histograms with a variance reduction higher than 80%. Variations in perovskite and in iron can be simultaneously incorporated (combinations 18 and 20), but lead to histograms close to those obtained for anomalies of temperature and perovskite alone. Combinations for which enrichment in perovskite is stronger than depletion in perovskite do not explain SB10L18 (combination 21). Similarly, the variance reduction decreases significantly (to 75%) if the amplitude of hot anomalies is stronger than that of cold anomalies (combination 27). Finally, in combination 28 we accounted for 0.1% (locally, 1–3%) of

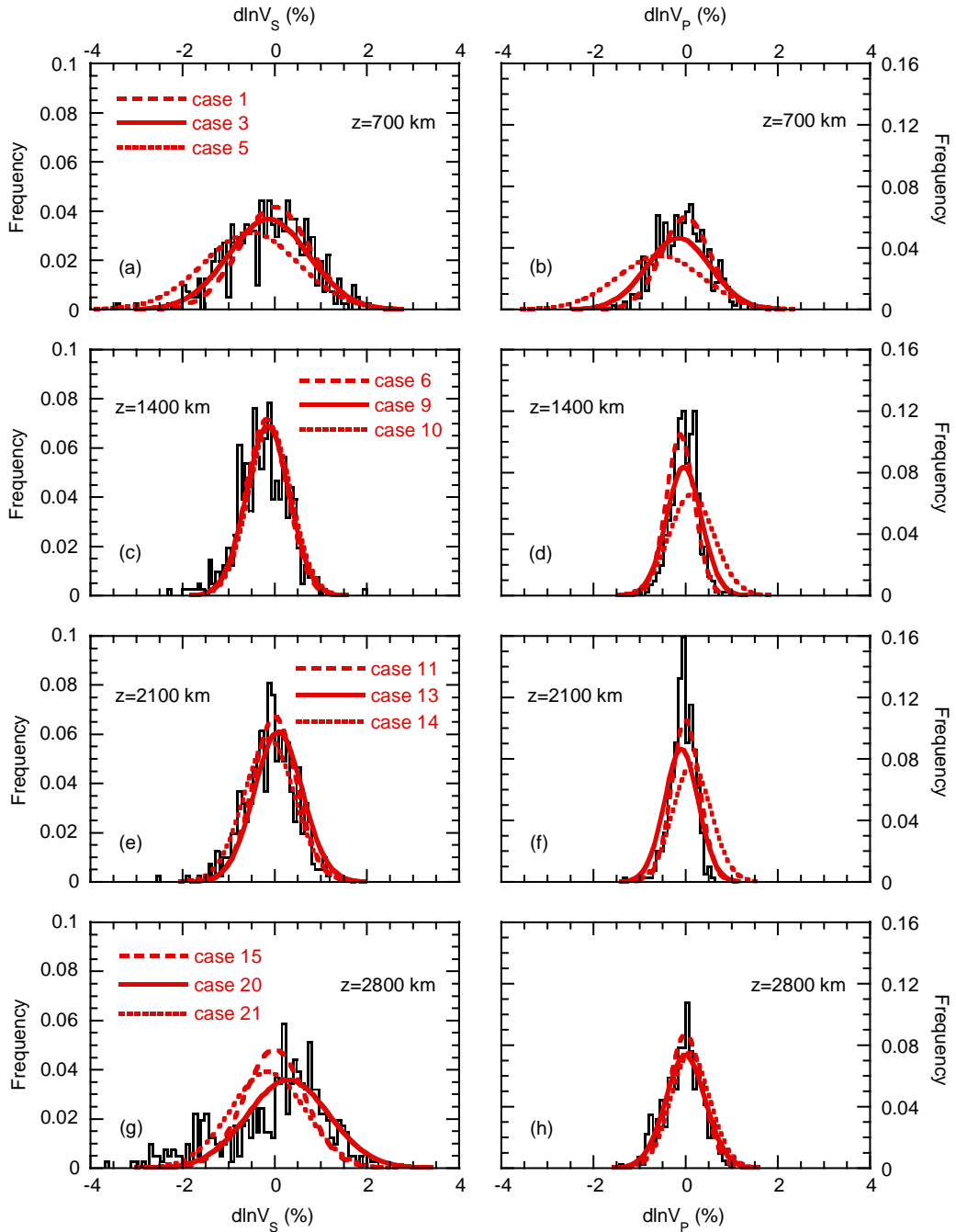


Fig. 7. Selected histograms (bold red curves) of relative V_S (left column) and V_P (right column) anomalies. The black curves represent the histograms for SB10L18. (a–b) $z = 700$ km, combinations 1, 3 and 5 in Table 4; (c–d) $z = 1400$ km, combinations 6, 9 and 10; (e–f) $z = 2100$ km, combinations 11, 13 and 14; (g–h) $z = 2800$ km, combinations 15, 20 and 21.

partial melt. A slightly different range of temperature variation is then required to fit SB10L18, but strong perovskite anomalies are still needed.

In the top and mid-lower mantle, the comparison between observed and synthetic histograms gives a relatively homogeneous image of the mantle. Temperature variations reach a maximum of ± 300 K. Local variations in the volumic fractions of perovskite and iron are possible, but limited in amplitude. At the bottom of the mantle, histograms clearly suggest the presence of strong chemical heterogeneities (as variations in the volumic fraction of perovskite), and possibly iron. Large lateral anomalies of temperature (up to 500 K) are likely at these depths. Although not all variations can be distinguished unambiguously, a robust feature is the need for regions with strong depletion (up to 14%) and enrichment (up to 10%) in perovskite. Variations in iron and/or the presence of partial melt still require strong variations in perovskite. Also robust is that the variations in iron, if present, should not exceed 2 to 3%.

The shape of histograms of velocity anomalies contains important information, since it is directly related to the distributions of anomalies of temperature and composition. Using average values of the ratio R , Karato and Karki (2001) argued for significant anelastic effects and a variety of chemical components at the bottom of the mantle. Full comparisons of synthetic and predicted histograms of velocity anomalies suggest that anomalies of temperature and perovskite (and possibly iron) are enough to explain the observations.

6. Importance of the density variations

As seen above, the distribution of R qualitatively suggests that temperature anomalies alone are not able to explain the observed histograms. The shape of the histograms of relative velocity anomalies provides quantitative constraints, but some trade-offs remain. To further constrain the analysis, we suggest that density distributions are needed.

The existence of trade-offs between anomalies of temperature and composition is not so surprising, given the nature of the sensitivities of velocity (Fig. 1). Accurate determinations of lateral variations of temperature and composition require the knowledge of the density distributions, because density has

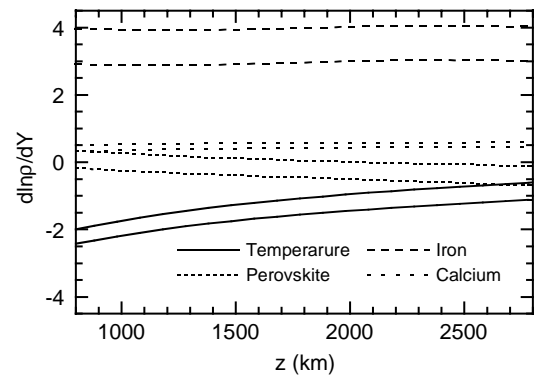


Fig. 8. Sensitivities of density to temperature ($\times 10^5$, plain curves), perovskite ($\times 10$, dotted curves), iron ($\times 10$, long dashed curves) and calcium ($\times 10$, short dashed curves) as a function of depth. In each case, we represent the upper and lower value of the sensitivity, which correspond to 1 standard deviation around the average. Averages and standard deviations are calculated from the predicted models that fit PREM within 1%.

a different sensitivity to composition than seismic velocities. The knowledge of density is particularly important for estimating iron anomalies in the upper (Forte and Perry, 2000; Deschamps et al., 2002) and lower mantle (Forte and Mitrova, 2001; Karato and Karki, 2001). The reason is that density is an increasing function of the volumic fraction of iron, whereas seismic velocities are decreasing functions of iron content. On the other hand, both density and seismic velocities decrease with increasing temperature.

We have explicitly computed sensitivities of density to temperature, perovskite, iron and calcium in the lower mantle (Fig. 8). Again, it is worth noting that throughout the mantle the sensitivity of density to calcium is very small compared to sensitivities to other parameters. Variations of Ca-Perovskite, if present, should not influence density anomalies. Throughout the mantle, the sensitivity of density to temperature is negative, whereas the sensitivity to iron is positive. This different behaviour of density with temperature and iron content is the reason why density anomalies can discriminate between anomalies of temperature and iron, the main trade-off. Although, the sensitivity of density to perovskite is similar to that of V_S , perovskite content is better determined simply because temperature and iron are tightly constrained.

A summary of the main properties of the different sensitivities in the lowermost ($z = 2000$ km) mantle

Table 5
General characteristic of sensitivities in the lowermost mantle ($z \geq 2000$ km)^a

	V_P		V_S		Density	
	Sign	Variation	Sign	Variation	Sign	Variation
Temperature	–	↓	–	↓	–	↓
Perovskite	+	↓	–	↑	–	↑
Iron	–	↓	–	↓	+	↑

^a For each sensitivity, two characteristics are listed: its sign, and the variation of its absolute value with depth. The descending arrow (↓) indicates a decreasing function of depth, and the ascending arrow (↑) indicates an increasing function of depth.

can be found in Table 5. Because each unknown temperature, perovskite and iron has a different signature, the analysis of $d \ln V_P$, $d \ln V_S$, and $d \ln \rho$ can determine temperature and the main compositional variations. Histograms of density anomalies are thus very important, since they are able to discriminate between the anomalies of iron and temperature. Mapping the density anomalies from normal modes is still controversial (Resovsky and Ritzwoller, 1999; Masters et al., 2000; Ishii and Tromp, 2001; Kuo and Romanowicz, 2002), but Resovsky and Trampert (2003) have recently proposed robust distributions of density anomalies using a neighbourhood algorithm. These distributions clearly indicate the presence of dense material at the bottom of the mantle. A preliminary comparison with synthetic histograms suggests that anomalies of iron could reach 3% in the lowermost mantle.

7. Conclusions

Distributions of velocity anomalies are, to date, the most detailed information concerning the thermal and chemical structure of the mantle. Directly inverting relative V_P and V_S anomalies for anomalies of temperature and composition within the uncertainties of current tomographic models and mineral physics data shows that compositional variations are not robust. Histograms of R , and in particular their dispersion, indicate qualitatively that the origin of V_P and V_S anomalies is not purely thermal, but also compositional. To estimate the range of temperature and compositional variations, we propose to use the histograms of the relative V_P and V_S anomalies. In the lowermost part of the mantle, this analysis suggests strong (from –14 to 10%) variations of perovskite and possible variations

in iron (from –1 to 2%). This result is in agreement with the model of Kellogg et al. (1999), where a dense layer (positive variations of perovskite) is displaced by descending slabs (negative variations of perovskite). The rest of the mantle can be explained by modest temperature variations alone, but chemical variations cannot be excluded. Several combinations of perovskite, iron and temperature anomalies fit the observed histograms equally well. This trade-off is likely to be broken by additional analysis of density variations.

Acknowledgements

We thank two anonymous reviewers for very helpful suggestions. This work was financed by the Geodynamics Institute at Utrecht University.

References

- Becker, T.W., Kellogg, J.B., O'Connell, R.J., 1999. Thermal constraints on the survival of primitive blobs in the lower mantle. *Earth Planet. Sci. Lett.* 171, 351–365.
- Beghein, C., Resovsky, J.S., Trampert, J., 2002. P and S tomography using normal-mode and surface waves data with a neighbourhood algorithm. *Geophys. J. Int.* 149, 646–658.
- Berryman, J.G., 2000. Seismic velocity decrement ratios for regions of partial melt in the lower mantle. *Geophys. Res. Lett.* 27, 421–424.
- Brodholt, J., Alfredsson, M., Price, D., 2003. Are computational mineral physics results accurate enough to detect chemical heterogeneity in the Earth's mantle? *Geophys. Res. Abs.* 5, abstract #7638, CD-ROM.
- Davaille, A., 1999. Simultaneous generation of hotspots and superswells by convection in a heterogeneous planetary mantle. *Nature* 402, 756–760.
- Deschamps, F., Trampert, J., Snieder, R., 2002. Anomalies of temperature and iron in the uppermost mantle inferred from gravity data and tomographic models. *Phys. Earth Planet. Inter.* 129, 245–264.

- Deschamps, F., Trampert, J., 2003. Towards a lower mantle reference temperature and composition. *Earth Planet. Sci. Lett.*, in press.
- Forte, A.M., Mitrovica, J.X., 2001. Deep-mantle high-viscosity flow and thermochemical structure inferred from seismic and geodynamic data. *Nature* 410, 1049–1056.
- Forte, A.M., Perry, A.C., 2000. Seismic–geodynamic evidence for a chemically depleted continental lithosphere. *Science* 290, 1940–1944.
- Garnero, E.J., Jeanloz, R., 2000. Fuzzy patches on the Earth's core–mantle boundary? *Geophys. Res. Lett.* 27, 2777–2780.
- Hammond, W.C., Humphreys, E.D., 2000. Upper mantle seismic wave velocity: effects of realistic partial melt geometries. *J. Geophys. Res.* 105, 10975–10986.
- Ishii, M., Tromp, J., 2001. Even-degree lateral variations in the Earth's mantle constrained by free oscillations and free-air gravity anomalies. *Geophys. J. Int.* 145, 77–96.
- Jackson, I., 1998. Elasticity, composition and temperature of the Earth's lower mantle: a reappraisal. *Geophys. J. Int.* 134, 291–311.
- Karato, S.-I., Karki, B.B., 2001. Origin of lateral variation of seismic wave velocities and density in the deep mantle. *J. Geophys. Res.* 106, 21771–21783.
- Karki, B.B., Crain, J., 1998. First-principles determination of elastic properties of CaSiO_3 perovskite at lower mantle pressures. *Geophys. Res. Lett.* 25, 2741–2744.
- Karki, B.B., Wentzcovitch, R.M., de Gironcoli, S., Baroni, S., 2000. High-pressure lattice dynamics and thermoelasticity of MgO . *Phys. Rev. B* 61, 8793–8800.
- Kellogg, L.H., Hager, B.H., van der Hilst, R.D., 1999. Compositional stratification in the deep mantle. *Science* 283, 1881–1884.
- Kennett, B.L.N., Engdahl, E.R., Bulland, R., 1995. Constraints on seismic velocities in the Earth from travel times. *Geophys. J. Int.* 122, 108–124.
- Knittle, E., Jeanloz, R., 1991. Earth's core–mantle boundary: results of experiments at high pressures and temperatures. *Sciences* 251, 1438–1443.
- Kuo, C., Romanowicz, B., 2002. On the resolution of density anomalies in the Earth's mantle using spectral fitting of normal-mode data. *Geophys. J. Int.* 150, 162–179.
- Labrosse, S., Tackley, P.J., 2001. Heat transfer by mantle convection in plate tectonics regime: preliminary 2D results, in: *Proceedings of the Seventh workshop on Numerical Modeling of Mantle Convection and Lithosphere Dynamics*, <http://link.springer.de/link/service/journals/10069/conferen/Aussois/index.html>.
- Marton, F.C., Cohen, R.E., 2002. Constraints on lower mantle composition from molecular dynamics simulations of MgSiO_3 perovskite. *Phys. Earth Planet. Inter.* 134, 239–252.
- Masters, G., Laske, G., Bolton, H., Dziewonski, A.M., 2000. The relative behavior of shear velocity, bulk sound speed, and compressional velocity in the mantle: implications for chemical and thermal structure, in: Karato, S.I., et al. (Ed.), *Earth's Deep Interior: Mineral Physics and Tomography from the Atomic to the Global Scale*, Geophysical Monograph Series, vol. 117. AGU, Washington, DC, pp. 63–87.
- Oganov, A.R., Brodholt, J.P., Price, G.D., 2001. Ab initio elasticity and thermal equation of state of MgSiO_3 perovskite. *Earth Planet. Sci. Lett.* 184, 555–560.
- Press, W.H., Flannery, B.P., Teukolsky, S.A., Vetterling, W.T., 1989. *Numerical Recipes*. Cambridge University Press, Cambridge, 702 pp.
- Resovsky, J.S., Ritzwoller, M., 1999. A degree 8 mantle shear velocity model from normal mode observations below 3 mHz. *J. Geophys. Res.* 104, 993–1014.
- Resovsky, J.S., Trampert, J., 2003. Using probabilistic seismic tomography to test mantle velocity–density relationships. *Earth Planet. Sci. Lett.* 215, 121–134.
- Revenaugh, J., Meyer, R., 1997. Seismic evidence of partial melt within a possibly ubiquitous low-velocity layer at the base of the mantle. *Science* 277, 670–673.
- Ringwood, A.E., 1991. Phase transformations and their bearing on the constitution and dynamics of the mantle. *Geochim. Cosmochim. Acta* 55, 2083–2110.
- Ritsema, J., van Heijst, H.-J., 2002. Constraint on the correlation of P- and S-wave velocity heterogeneity in the mantle from P, PP, PPP and PKPab traveltimes. *Geophys. J. Int.* 149, 482–489.
- Robertson, G.S., Woodhouse, J.H., 1997. Comparison of P- and S-station corrections and their relationship to upper mantle structure. *J. Geophys. Res.* 102, 27355–27366.
- Saltzer, R.L., van der Hilst, R.D., Káráson, H., 2001. Comparing P and S wave heterogeneity in the mantle. *Geophys. Res. Lett.* 28, 1335–1338.
- Sinelnikov, Y.D., Chen, G., Neuville, D.R., Vaughan, M.T., Liebermann, R.C., 1998. Ultrasonic shear wave velocities of MgSiO_3 perovskite at 8 GPa and 800 K and lower mantle composition. *Science* 28, 677–679.
- Sinogeikin, S.V., Bass, J.D., 1999. Single crystal elasticity of MgO at high-pressure. *Phys. Rev. B* 59, 14141–14144.
- Su, W.-J., Dziewonski, A.M., 1997. Simultaneous inversion for 3D variations in shear and bulk velocity in the mantle. *Phys. Earth Planet. Inter.* 100, 135–156.
- Sumino, Y., Anderson, O.L., Suzuki, I., 1983. Temperature coefficients of elastic constants of single crystal MgO between 80 and 1300 K. *Phys. Chem. Mineral.* 9, 38–47.
- Trampert, J., Vacher, P., Vlaar, N., 2001. Sensitivities of seismic velocities to temperature, pressure and composition in the lower mantle. *Phys. Earth Planet. Inter.* 124, 255–267.
- Wang, Y., Weidner, D.J., Guyot, F., 1996. Thermal equation of state of CaSiO_3 perovskite. *J. Geophys. Res.* 101, 661–672.
- Williams, Q., Garnero, E.J., 1996. Seismic evidence of partial melt at the base of the mantle. *Science* 273, 1528–1530.